ACS OMEGA

Open Access

http://pubs.acs.org/journal/acsodf

Article

Hydrogel Composite Incorporating Deferoxamine-Loaded Gelatin-Based Microspheres Enhance Angiogenesis Ability of Dental Pulp Stem Cells

Jie Wang, Fan Yang, Ruting Chen, Xinyue Yang, Jingjing Wang, and Hongyan Zhang*

Cite This: *ACS Omega* 2025, 10, 12579−12589

Read Online

ACCESS | Metrics & More | Article Recommendations

ABSTRACT: Fast reconstruction of the pulpal vasculature is crucial for effective pulp regeneration. Dental pulp stem cells (DPSCs) are promising candidates for pulp regeneration because of their potential for multilineage differentiation and vasculogenic properties. Deferoxamine (DFO) has been shown to stimulate angiogenesis during wound healing and bone regeneration; however, the effects of DFO on the angiogenic potential of DPSCs remain unknown. Moreover, its usefulness is restricted by a limited half-life and challenges in achieving localized tissue enrichment. This study aimed to develop a sustained-release injectable hydrogel composite as a drug delivery system and to investigate its influence on DPSCs. Herein, gelatin-based microspheres (GMSs) were loaded with DFO, and temperature-sensitive injectable hydrogels incorporating collagen and chitosan were synthesized to enable controlled DFO release. The experimental findings demonstrated that the DFO-loaded GMSs (DFO-GMSs) hydrogel composite possessed favorable physical properties and biocompatibility, enabling sustained DFO delivery for up to 15 days. DFO effectively stimulated DPSC migration, promoted the secretion of angiogenesis-related factors, and induced tube formation in vitro. These results suggest that the DFO-GMSs hydrogel composite significantly increased the migration and angiogenic potential of DPSCs, highlighting its promise for tissue regeneration applications.

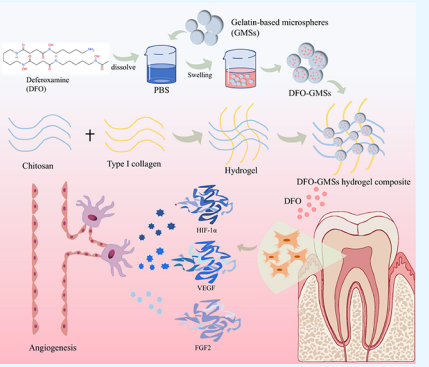

1. INTRODUCTION

Dental pulp is characterized by a high degree of vascularization. The pulp within the root canal is surrounded by dentin under normal conditions, relying on the narrow apical foramen for nutrient intake and metabolic exchange. In the context of pulp regeneration, however, the tissue must reconstruct its vascular network and restore blood circulation exclusively through the restricted apical foramen.[1] Rapid reconstruction of pulpal vasculature is considered critical for successful pulp regeneration.[2] Dental pulp stem cells (DPSCs), the progenitors of dental pulp cells, are considered the primary candidates for pulp regeneration and are required to have strong angiogenic capabilities.[3−5] Therefore, DPSCs and angiogenesis-related growth factors are frequently integrated into pulp tissue engineering to facilitate efficient pulp regeneration.[6−9]

The iron chelator deferoxamine (DFO) is used to treat iron toxicity and is also extensively employed for hypoxia induction.[10,11] In recent years, DFO has also been used in regenerative medicine, as it reduces inflammation and enhances angiogenesis in bone regeneration.[12−15] Recent studies have demonstrated that DFO can activate the TGF-β1/Smad2 axis to promote bone formation and induce mesenchymal stem cell (MSC) differentiation.[16,17] Furthermore, DFO can also effectively inhibit proline hydroxylase (PHD), preventing proline hydroxylation of HIF-1α. This inhibition effectively activates the HIF-1α axis, leading to the upregulation of angiogenesis promoters, including the downstream mediator VEGF, and promoting neointima formation.[18,19] However, the use of DFO is restricted by its limited half-life, necessitating the administration of multiple doses to achieve an effective drug concentration. Moreover, it is challenging to concentrate the drug in localized tissues when administered orally or via intraperitoneal injection.[20] The application of macromolecular iron chelators, such as nanogels, has been shown to enhance DFO pharmacokinetics, ensuring better-localized drug enrichment and sustained release at target sites.[21−23]

In pulp regeneration, DFO can promote dental pulp cells (DPCs) migration and odontogenic differentiation, supporting tissue repair and regeneration processes.[25,26] Furthermore,

Received: January 15, 2025
Revised: March 3, 2025
Accepted: March 14, 2025
Published: March 21, 2025

DFO has been recognized for its potential to stimulate the osteogenic differentiation of human periodontal ligament cells (hPDLCs).[24] Lee et al. demonstrated that DFO reduced inflammation and osteoclast formation in vitro, while also decreasing bone resorption in a rat tooth replantation model.[27] However, studies exploring the combination of DFO with slow-release systems to evaluate its impact on DPSCs are limited.

This study aimed to design an injectable drug delivery system with a slow drug release profile while providing an environment supportive of DPSCs adhesion, proliferation, and differentiation. Gelatin-based microspheres (GMSs), recognized for their remarkable malleability, can serve as effective drug carriers for the delivery of bioactive molecules.[28,29] Hydrogels are comprised of hydrophilic polymers that are cross-linked either physically or chemically, forming a 3D network structure. The described structure allows them to efficiently encapsulate and release active compounds and biomolecules.[30] Chitosan is an extensively used hydrogel material that possesses temperature sensitivity when combined with sodium glycerophosphate. It remains liquid at room temperature and solidifies upon reaching physiological temperature (37 °C), making it an ideal candidate for effective use as an injectable scaffold.[31] Furthermore, Type I collagen represents the primary constituent of bone extracellular matrix. It is characterized by low immunogenicity and higher biocompatibility, facilitating osteogenesis and mineralization.[32,33]

In summary, synthesis of GMSs was undertaken using the emulsion-solvent extraction method, with subsequent loading of DFO to enable controlled drug release. A hydrogel was developed by combining chitosan and type I collagen, encapsulating the microspheres to further regulate DFO release while also providing an optimal environment for DPSCs. The developed system, referred to as the DFO-GMSs hydrogel composite, has been investigated through in vitro experiments to assess its effects on DPSCs. Hence, it is anticipated that this system will inspire new approaches in endodontic regenerative therapy.

2. MATERIALS AND METHODS

2.1. Preparation of DFO-GMSs Hydrogel Composite.

2.1.1. Fabrication of GMSs. The fabrication of GMSs was carried out using the Nouri-Felekori modified method.[34] Briefly, 2.5 g of gelatin (G108395, Aladdin, Shanghai, China) was placed in 25 mL of deionized water and heated at 50 °C for 30 min prior to the incorporation of 1.25 mL of cross-linker GPTMS (D834054, Macklin, Shanghai, China). The mixture was then stirred for 2 h at 500 rpm and was then gradually introduced to 125 mL of olive oil and incubated with stirring at 40 °C for 24 h to form GMSs. After that, 50 mL of precooled isopropanol was incorporated, and the mixture was stirred to promote dehydration. Filtration was carried out to collect the GMSs, which were subsequently washed with 1 L of isopropanol. The collected GMSs were freeze-dried and subjected to ultraviolet irradiation for 24 h.

2.1.2. Preparation of DFO-GMSs. The swellable property of GMSs was used to load the DFO according to established methods.[59,60] The small molecular size of DFO enables its penetration into swollen hydrogel matrices through concentration gradient-driven diffusion.[65] Additionally, the abundant amide groups in both DFO and the gelatin-based hydrogel facilitate hydrogen bonding interactions, which synergistically enhance drug adsorption and loading efficiency within the polymeric network.[66,67] In essence, 2.5 mL of DFO (Y0001937, Sigma-Aldrich, Missouri, USA) in PBS was incorporated into 1 g of GMSs at varying concentrations of 0, 10, 20, 40, and 80 μM. The solution was then gently mixed with the microspheres to ensure uniform absorption of the drug and resulting DFO-GMSs were freeze-dried for 48 h. The samples were labeled as DFO-0, DFO-10, DFO-20, DFO-40, and DFO-80, corresponding to the respective concentrations.

2.1.3. Fabrication of DFO-GMSs Hydrogel Composite. For the preparation of chitosan-β-glycerophosphate solution, 0.2 g of chitosan (C434553, Aladdin, Shanghai, China) powder was exposed to ultraviolet irradiation for 2 h. The irradiated chitosan was then added to 10 mL of glacial acetic acid (0.1 mol/L) and stirred at 600 rpm for 3 h until fully dissolved. After that 45% β-glycerophosphate (Solarbio, Beijing, China) solution was filtered (0.22 μm) for removal of bacteria. While maintaining an ice bath, 2.5 mL of the filtered β-glycerophosphate solution was slowly incorporated into the chitosan solution followed by 2 h stirring to obtain the chitosan-β-glycerophosphate solution. In an ice bath, 2 mL of type I rhamnogelatin solution (1 g/L, Solarbio, Beijing, China) was introduced to 12.5 mL of the chitosan-β-glycerophosphate solution and mixed well, resulting in the formation of a temperature-sensitive chitosan-collagen composite hydrogel. Following this, different DFO-GMSs (400 mg) were added to 1 mL of the liquid hydrogel composite to develop different DFO-GMSs hydrogel composites.

2.2. DFO-GMSs Hydrogel Composite Morphology. SEM (GeminiSEM 300, Carl Zeiss) was utilized to evaluate the structures of the DFO-GMSs, hydrogel alone, and DFO-GMSs hydrogel composites at magnifications of 100× and 1000×. The freeze-dried samples were mounted on aluminum stubs followed by coating with gold. More than 200 drug-loaded microspheres from SEM images were randomly selected while the size of the microspheres was measured using ImageJ software and the particle size distribution was analyzed using Origin software. Furthermore, the DFO-GMSs hydrogel composite was immersed in PBS, and images were captured daily using a Leica microscope (M205FA, 402313, Singapore) until the complete degradation of drug-loaded microspheres. Each experiment was conducted in triplicate.

2.3. In Vitro Release of the DFO-GMSs Hydrogel Composite. The cumulative DFO release from GMSs, hydrogel, and GMSs hydrogel composites was determined by Ultraviolet spectrophotometry (UV-1800, Shimadzu, Kyoto, Japan). Briefly, DFO-loaded hydrogels (1 mL), DFO-GMSs (400 mg), and DFO-GMSs hydrogel composites (1 mL) were separately immersed in 5 mL of PBS. A 0.3 mL aliquot of the supernatant was collected to measure the drug content. To assess DFO concentration, ferric chloride ($FeCl_3$, 0.1 mol/L) was added to the supernatant, as the DFO-Iron III chelate complex has a maximum absorbance at 430 nm. The DFO concentration was determined using UV-1800 at 430 nm, and the drug concentrations were calculated with reference to a standard curve. The calculation equation can be written as follows:

$$\text{Cumulative drug release (\%)} = \frac{\text{Released drug at each time point}}{\text{Total quantity of loaded drug}} \times 100\%$$

https://doi.org/10.1021/acsomega.5c00445
ACS Omega 2025, 10, 12579−12589

The results are presented as mean ± standard deviation, with each group undergoing three independent experiments.

2.4. Rheological Assay. The DFO-GMSs hydrogel composites and hydrogel alone were evaluated for their rheological properties using a rheometer (MCR 302e, Anton Paar). Changes in the loss modulus (G'') and storage modulus (G') were recorded over frequencies of 1−100 Hz, and the data were plotted as line graphs. From each group, three different specimens were analyzed.

2.5. Compression Test. DFO-GMSs hydrogel composite and hydrogel alone were solidified at 37 °C. Compression tests were performed on all specimens using a mechanical tester (AGS-X, Shimadzu, Kyoto, Japan) at a rate of 3 mm/min. Stress−strain curves were formed within the strain range of 0−70%, and the compression modulus was then determined using the slope of the curve. Three different specimens were characterized from each group.

2.6. Isolation and Culturing of DPSCs. DPSCs were harvested from freshly extracted human teeth (healthy donors aged 18−30 years) following approval from the Ethics Committee (T2024037). Briefly, the collected pulp tissues were minced and digested with the help of 3 mg/mL collagenase type I (Solarbio, Beijing, China) for 45 min at 37 °C. The digestion was terminated by the addition of a complete medium containing fetal bovine serum and centrifugation (1000 rpm, 5 min). The cell pellets were seeded into a six-well plate, pressing with a coverslip to facilitate cell release. αMEM (Gibco, Grand Island, USA) containing 2% antibiotic-antimycotic(Beyotime, Shanghai, China) and 20% fetal bovine serum (Wisent, Nanjing, China) was added, and cells were grown at 37 °C with 5% CO_2. Cells were subcultured when 80% confluent, and third to sixth generation cells were used for further investigation.

2.7. Flow Cytometry. Following cell digestion, 2×10^5 cells/100 μL were treated with antibodies against CD34, CD14, CD90, and CD73 (2 μL of each, Biolegend, America), with incubation for 30 min at 4 °C. The cells were washed three times with PBS (3 mL), followed by 5 min centrifugation at 1000 rpm. The cells were suspended in PBS (200 μL) for subsequent flow cytometry analysis using flow cytometer (CytoFlex, Beckman, USA).

2.8. Live/Dead Experiment. Under sterile conditions, 1 mL of GMSs hydrogel composite was prepared and inoculated into each well of a 24-well plate. DPSCs (3×10^4 cells per well) were then seeded onto the composite surface and allowed to culture for 24, 72, and 120 h. After removal of the medium, the cells were washed once using PBS. The Calcein/PI Cell Viability Assay Kit (C2015, Beyotime, Shanghai, China) was employed to assess cell viability. The working solution contained 2 mL of assay buffer, 1 μL of Calcein AM (1000×), and 1 μL of PI (1000×) and 250 μL of this were placed in each well, followed by incubation at 37 °C for 30 min in the dark. After being incubated, the staining effect was determined using an automatic intelligent fluorescence microscope (DM6000B, Leica, Germany). All experiments were repeated in triplicate.

2.9. Morphological Observation of DPSCs. Onto the samples, DPSCs (3×10^4 cells) were seeded and allowed to culture for 1, 3, and 5 days. Cells were fixed with 4% glutaraldehyde for 30 min at room temperature. F-actin in the cytoskeleton was stained with FITC-phalloidin (Solarbio, Beijing, China) for 30 min, while the nuclei were counterstained with DAPI (Solarbio, Beijing, China) for 5 min. Morphology was evaluated using a confocal laser scanning microscope (Celldiscoverer, ZEISS, Germany).

2.10. Cell Proliferation Assay. DPSCs (8000/well) were seeded onto the DFO-GMSs hydrogel composites and grown for 24, 72, 120 h, after which CCK-8 solution (Biosharp, Tianjin, China) was added to each well according to the instructions. Cells are grouped by concentration: control, DFO-0, DFO-10, DFO-20, DFO-40 and DFO-80. After 2 h incubation, a microplate reader (Infinite 200 PRO, 30050303, Austria) was utilized for recording absorbances at 450 nm. Each experiment was performed in triplicate.

2.11. Scratch Wound Healing Assay. The influence of the DFO-GMSs hydrogel on DPSC migration was assessed using Transwell chamber. In a 24-well plate, DPSCs (5×10^4 cells/well) were inoculated in the lower chamber. Once the cells reached confluence, a scratch was introduced into the cell layer using a sterile pipet tip, forming a linear wound to assess cell migration. Each well was subjected to thrice washing with PBS and the upper chamber was filled with DFO-GMSs hydrogel composite. Images were recorded at 0 and 24 h from three random fields using a microscope (DMI3000B, Leica, Germany). Cell migration across the wound area was quantified by a single investigator, and experiments were conducted in triplicate to ensure consistency.

2.12. Tube Formation Assay. Before the experiment, the Matrigel matrix (Corning, New York, USA) was prechilled at 4 °C for 24 h. Under sterile, ice-cold conditions, 300 μL of Matrigel was carefully incorporated into each well of a precooled 24-well plate, ensuring no air bubbles were introduced, followed by incubation at 37 °C for 30 min to allow matrix solidification. After that, 3×10^4/well human umbilical vein endothelial cells (HUVECs; IM-H205, Immo Biotech, Xiamen, China) were inoculated onto the Matrigel. Supernatants from DPSCs treated with GMSs hydrogel composites for 48 h, containing varying concentrations of DFO, were incorporated into various experimental groups (DPSC groups), while supernatants from untreated DPSCs were used as controls (un-DPSC groups). Tube formation was assessed and recorded after 12 h of incubation using a microscope (DMI3000B, Leica, Germany). For each group, the relative lengths and numbers of tubules were quantified in three randomly selected fields of each sample using ImageJ software.

2.13. Enzyme-Linked Immunosorbent Assay (ELISA). In a 24-well plate, 1 mL of DFO-GMSs hydrogel composite (Control, DFO-0, DFO-10, DFO-20, DFO-40) was placed and DPSCs (3×10^4 cells/well) were inoculated onto the hydrogel surface and cultured for 48 h. For ELISA experiments, Human FGF-2 ELISA Kit (HJ243, Epizyme Biomedical, Shanghai, China), Human VEGF ELISA Kit (HJ115, Epizyme Biomedical, Shanghai, China), and Human Total HIF-1α ELISA Kit (EK1392, LiankeBio, Hangzhou, China) were used to analyze secretory VEGF, FGF-2, and HIF-1α. Absorbances at 450 nm were recorded in a microplate reader as above and the actual concentrations were determined relative to a standard curve.

2.14. Quantitative Realtime Polymerase Chain Reaction (qPCR). A Transwell chamber was utilized to assess the effect of different concentrations of DFO released from GMSs hydrogel composites on DPSCs. DPSCs (3×10^4 cells/well) were inoculated in the lower chamber in a 24-well plate and growth for 48 h, while the DFO-GMSs hydrogel composites were capped with the upper chamber. Total RNA was

https://doi.org/10.1021/acsomega.5c00445
ACS Omega 2025, 10, 12579−12589

Table 1. qPCR Primer Sequences

gene	forward	reverse
VEGF	5′-CAAAAACGAAAGCGCAAGAAA-3′	5′-GCGGGCACCAACGTACAC-3′
FGF2	5′-GCTGTACTGCAAAAACGGGG-3′	5′-CTTTCTGCCCAGGTCCTGTT-3′
HIF-1α	5′-GAACGTCGAAAAGAAAAGTCTCG-3′	5′-CCTTATCAAGGATGCGAACTCACA-3′
ACTN	5′-GGCATGGACTGTGGTCATGAG-3′	5′-TGCACCACCAACTGCTTAGC-3′

extracted using RNA-Quick Purification Kit (YiShan Biotech, Shanghai, China) and used for cDNA synthesis using the HifairII first Strand cDNA Synthesis Kit (YESEN, Shanghai, China). qPCR was performed using the Agilent Mx3000P with SYBR green. Reactions were comprised of 1 cycle of 95 °C for 5 s and 40 cycles of 95 °C for 5 s, 60 °C for 30 s. The primers are shown in Table 1. Gene expression levels were analyzed using the ΔΔCT method, with expression of target genes relative to the controls. Expression values were normalized to ACTIN expression levels.

2.15. Statistical Analysis. All experiments were repeated three times and all data were expressed as mean ± standard deviation (SD). Data from multiple groups were analyzed using one-way or two-way analysis of variance (ANOVA). Results were considered significant with p-values below 0.05 ($^{*}p < 0.05$, $^{**}p < 0.01$, $^{***}p < 0.001$).

3. RESULTS

3.1. Characterization of DFO-GMSs Hydrogel Composite. The freeze-dried DFO-GMSs displayed a complete and regular spherical morphology as shown in Figure 1A. The results of particle size distribution showed that the microsphere diameters were mainly distributed in the range of 20−100 μm, with more than 70% of the microspheres concentrated in the smaller interval of 30−60 μm (Figure 1E). Furthermore, the hydrogel demonstrated a porous structure, with the microspheres encapsulated within the pores. The temperature-sensitive characteristics of DFO-GMSs hydrogel composite are depicted in Figure 1B. It was observed that the hydrogel remained in the liquid phase at 4 °C, but became solid when incubated for 30 min at 37 °C. Upon soaking in PBS for 24 h, the DFO-GMSs retained their smooth and intact spherical shape, while only partial gelatin debris was observed after 35 days.

Throughout the 0.1−100 rad/s frequency range, the storage modulus (G′) surpassed the loss modulus (G″), indicating that both the hydrogel and GMSs hydrogel composite maintained a solid-like state under both low and high-frequency conditions. The observed finding suggests that neither material transitioned from a solid-like state to a fluid state during the scanning process (Figure 1D).

The stress−strain curve revealed that the DFO-GMSs hydrogel composite group demonstrated a higher modulus of elasticity than the composite hydrogel group. The material demonstrated a tensile strength of 20 kPa at a strain of 70%, indicating that it possesses sufficient structural strength for use in brackets. These findings suggest that the hydrogel maintained a stable state with improved mechanical properties (Figure 1C).

In the in vitro experiments, drug release was measured using a spectrophotometer (Figure 1F). The results indicated that the hydrogel alone released the drug over the shortest duration, while the GMSs hydrogel composite demonstrated the longest release period, extending up to 15 days. At the initial stage (0−5 days), a rapid release of the drug was observed, primarily due to the rapid degradation of the drug-loaded microspheres located on the surface and in the shallow layers of the hydrogel. This phenomenon leads to a burst release of the drug. Over time, the encapsulated drug was gradually released through the hydrogel's pores, leading to a sustained and gradual release rate.

3.2. Influence of DFO-GMSs Hydrogel Composite on DPSC Viability. DPSCs were successfully isolated and cultured, and flow cytometry analysis confirmed their positivity for mesenchymal markers CD90 and CD73, while they were found to be negative for hematopoietic markers CD14 and CD34 (Figure 2A).

Early cell adhesion is important for subsequent cell growth and differentiation, directly influencing biological behavior.[35] A live/dead assay was performed to assess the biocompatibility of the materials and evaluate their effect on cell morphology. In this assay, green fluorescence represents living cells, while red fluorescence denotes dead cells. As shown in Figure 2B, the hydrogel and GMSs hydrogel composite groups showed predominantly green fluorescence, with minimal red fluorescence, indicating good cell viability. After 5 days of cell culture, significant proliferation of DPSCs was observed within the hydrogel composite. However, no marked variation was found in cell growth between the hydrogel and GMSs hydrogel composite groups at the three distinct time points. To further evaluate the ability of GMSs hydrogel composite to promote cell adhesion, spreading, and growth, DPSCs were seeded on different groups of hydrogels and stained. In Figure 2C, on day 1, DPSCs adhered to the GMSs hydrogel composite and appeared circular. Over time, their morphology gradually changed, and by day 5, the cells displayed a more elongated, spindle-like, and polygonal shape, indicating successful cellular contact. The findings indicated that the DFO-GMSs hydrogel composite possessed significant biocompatibility and could support the adhesion and proliferation of DPSCs.

Figure 2D shows the viability of DPSCs at varying concentrations of DFO, which were assessed to identify the optimal concentration for further experiments. No marked differences in viability were observed between the control group and cells treated with various DFO concentrations at day 1 ($p > 0.05$). However, after 3 days, the DFO-80 group showed markedly decreased DPSC viability ($p < 0.05$). After 5 days, cell survival in the DFO-80 group was significantly lower upon comparison with the control group, while survival increased in the DFO-10 group ($p < 0.05$). According to the observed results, DFO-10, DFO-20, and DFO-40 concentrations were used for further investigations.

3.3. DFO-GMSs Hydrogel Composite Promoted DPSC Migration. To examine the effects of the DFO-GMSs hydrogel composite on DPSC migration, scratch wound healing assays were conducted, finding that DFO treatment markedly increased DPSC migration relative to the controls ($p < 0.05$). The DFO-treated groups, especially DFO-20 and DFO-40, demonstrated more pronounced migration toward the wound (Figure 3A).

https://doi.org/10.1021/acsomega.5c00445
ACS Omega 2025, 10, 12579−12589

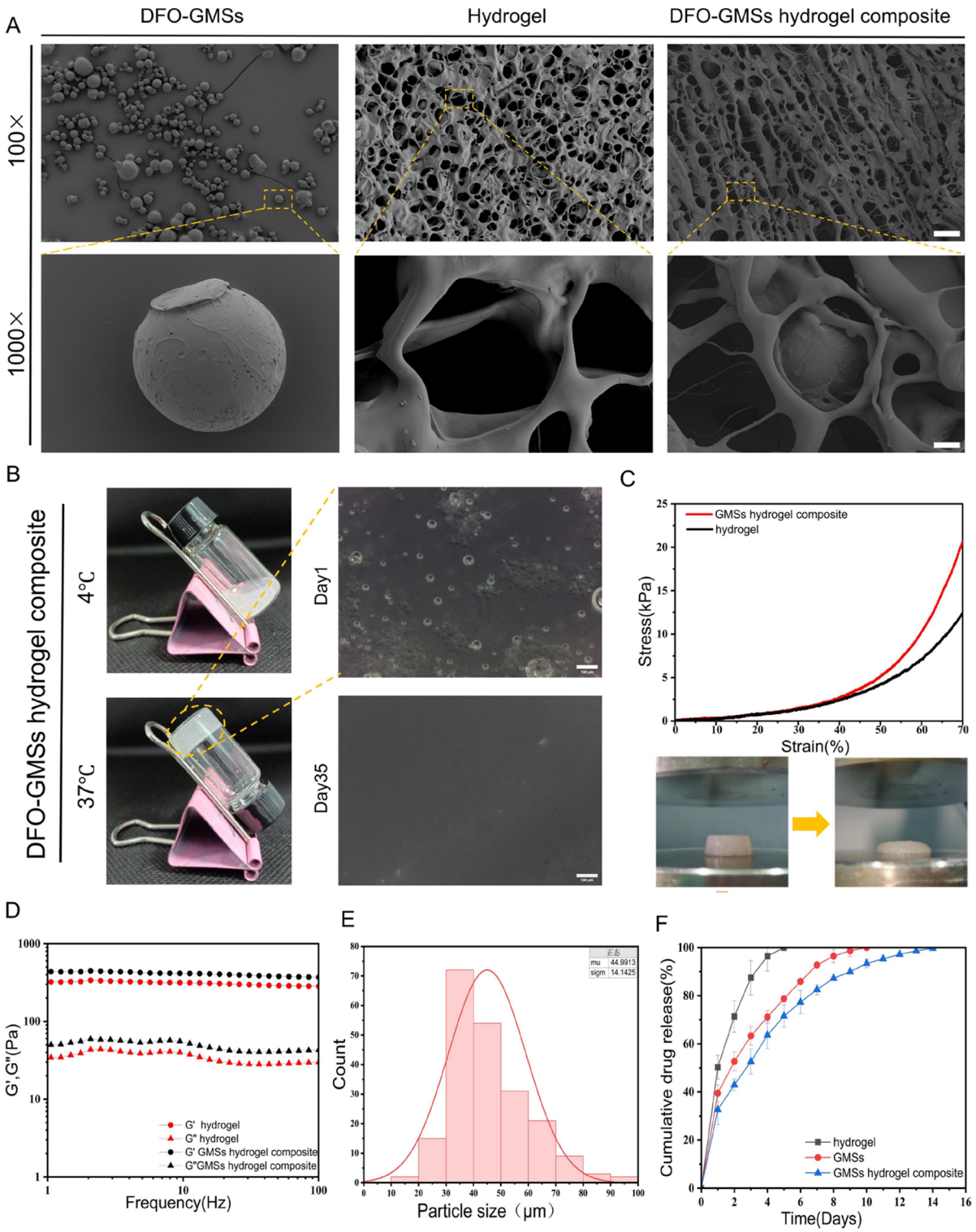

Figure 1. Characterization of DFO-GMSs hydrogel composite. (A) SEM images of hydrogel, DFO-GMSs, and DFO-GMSs hydrogel composite in low and high magnification. (B) The transition of GMSs hydrogel composite and hydrogel from 4 to 37 °C and optical images of DFO-GMSs hydrogel composite immersed in PBS on days 1 and 35. (C) Compression assay and (D) rheological analysis of GMSs hydrogel composite and hydrogel, $n = 3$. (E) Particle size distribution of DFO-GMSs. (F) Cumulative drug release behavior obtained from GMSs, hydrogel, and DFO-GMSs hydrogel composite in vitro, $n = 3$. Values are presented as the mean ± SEM. Scale bar: (A) low magnification = 100 μm, high magnification = 10 μm. (C) = 100 μm.

3.4. DFO-GMSs Hydrogel Composite Promoted Angiogenesis In Vitro. ELISA results showed the significantly higher secretion of VEGF, FGF2, and HIF-1α in DPSCs belonging to DFO-GMSs hydrogel composite group relative to both the GMSs hydrogel composite group and the controls ($p < 0.05$). The results revealed that DFO-GMSs hydrogel composite promoted the secretion of angiogenesis-related factors in DPSCs. Furthermore, higher concentrations of DFO

https://doi.org/10.1021/acsomega.5c00445
ACS Omega 2025, 10, 12579−12589

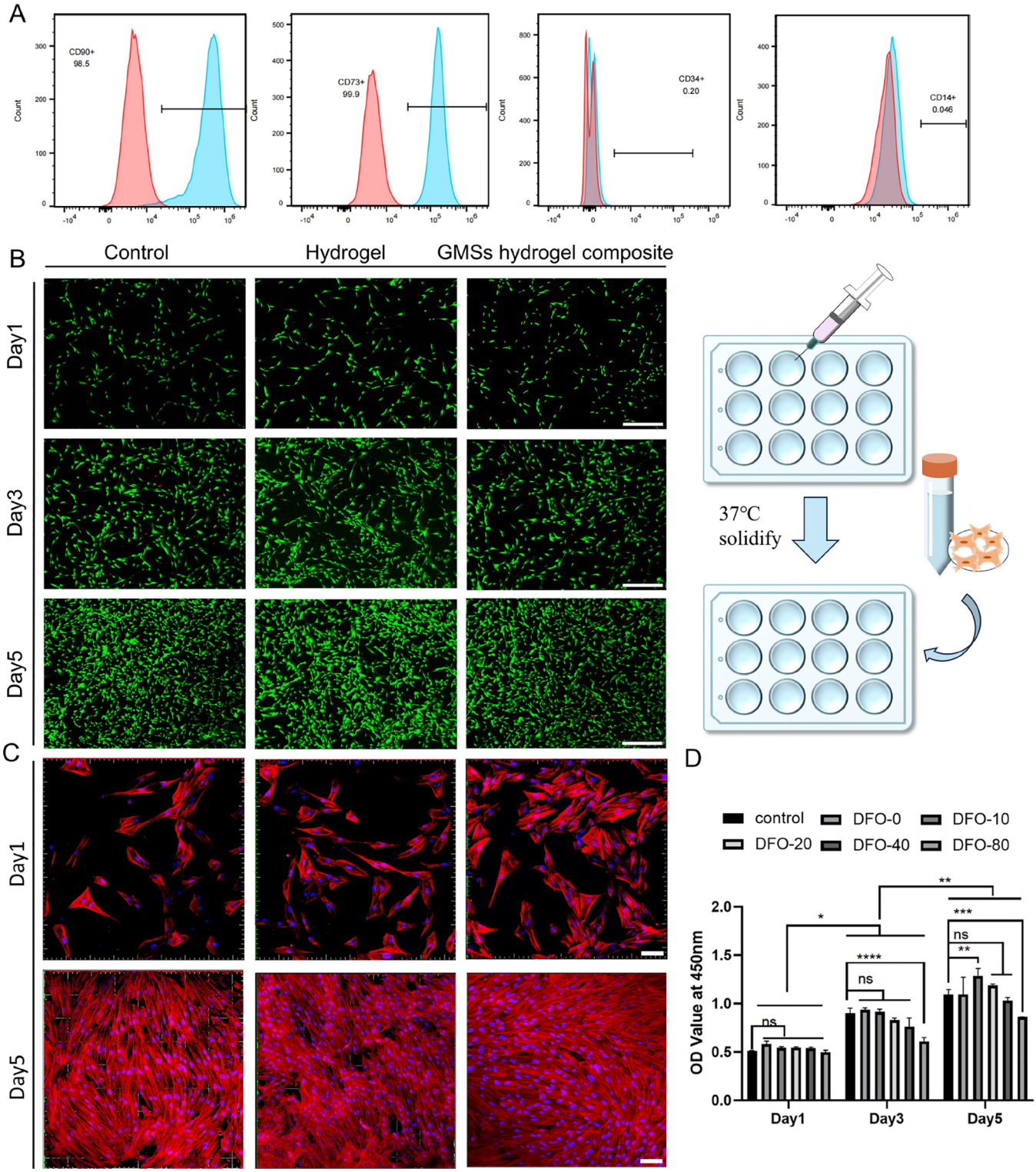

Figure 2. Influence of DFO-GMSs hydrogel composite on DPSC viability. (A) Flow cytometry analysis of specific markers on DPSCs. (B) Live/dead staining for Calcein AM and PI in Control-DPSC, Hydrogel-DPSC, and GMSs hydrogel composite-DPSC at 1, 3, and 5 days. (C) Cytoskeletal fluorescence staining of DPSCs after 1 and 5 days. (D) Viabilities at 1, 3, and 5 days after DPSC seeding, *$p < 0.05$. **$p < 0.01$. ***$p < 0.001$. ****$p < 0.0001$, ns $p > 0.05$. Scale bar: (B) = 500 μm. (C) = 100 μm.

(DFO-40) demonstrated a more pronounced effect. On the other hand, no marked differences were observed between the DFO-0 and control groups ($p > 0.05$), indicating that it is released DFO from GMSs hydrogel composite leads to this result (Figure 4C).

To further verify whether the DFO released from the hydrogel affects DPSCs, alterations in the levels of angiogenesis-related genes were examined using a Transwell chamber (Figure 4D). The results revealed that DFO enhanced secretion of VEGF, FGF2, and HIF-1α from

https://doi.org/10.1021/acsomega.5c00445
ACS Omega 2025, 10, 12579−12589

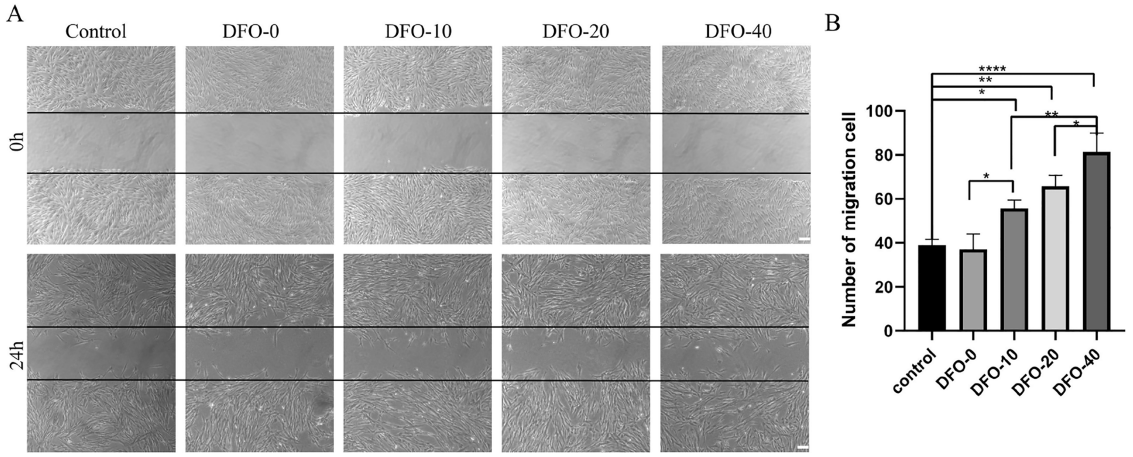

Figure 3. (A) Scratch wound healing assay and (B) number of migrated cells in relation to different DFO concentrations, $n = 3$. *$p < 0.05$. **$p < 0.01$. ***$p < 0.001$. ****$p < 0.0001$, ns $p > 0.05$. Scale bar: 200 μm.

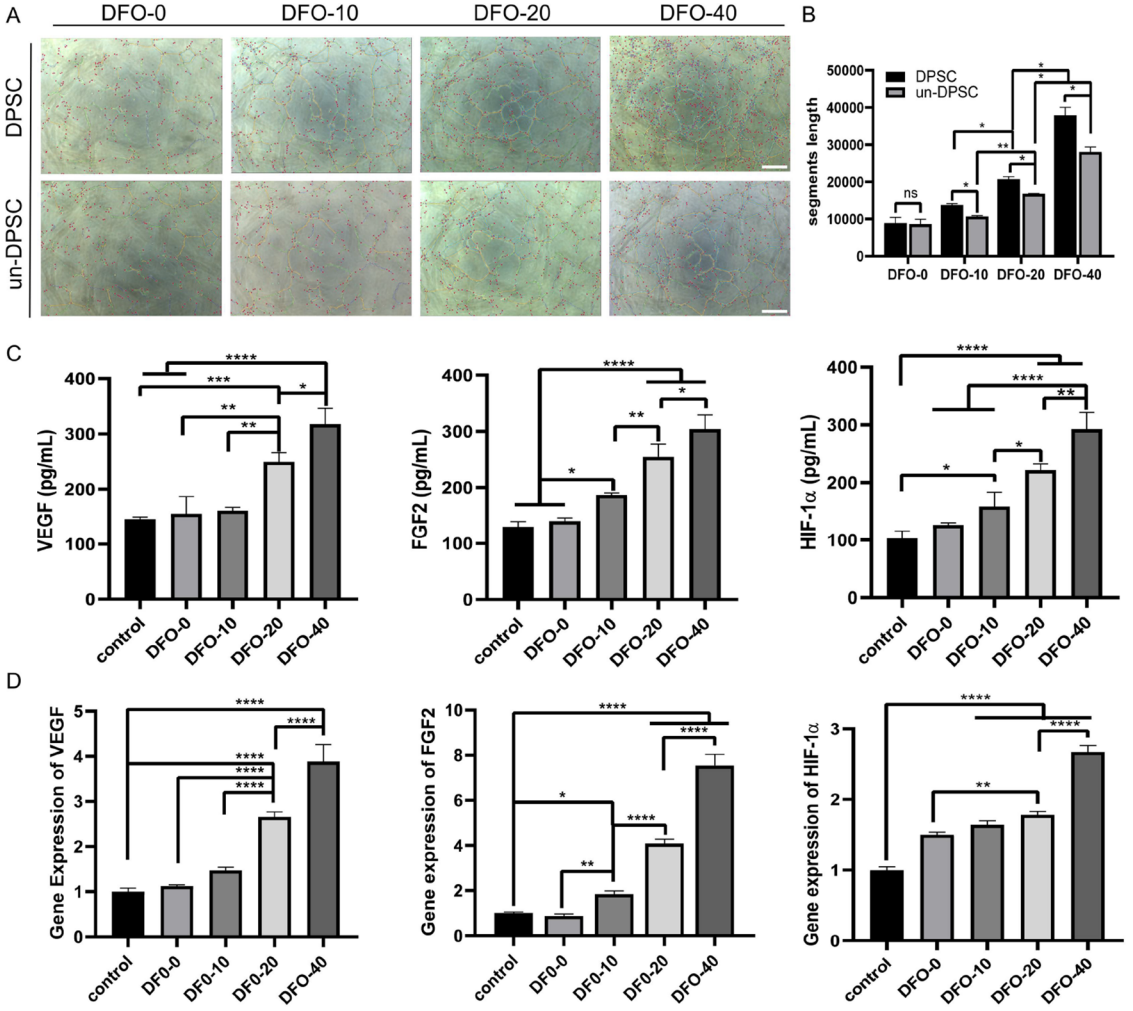

Figure 4. Effects of DFO-GMSs hydrogel composite on the angiogenic capacity of DPSCs in vitro. Tube formation assay (A) and quantification of (B) segment length under different concentrations of DFO, $n = 3$. Effects of DFO-GMSs hydrogel composite on levels and secretion of vascular-related factors (HIF-1α, VEGF, FGF2) in DPSCs as demonstrated by ELISA (C) and qPCR (D), $n = 3$. *$p < 0.05$. **$p < 0.01$. ***$p < 0.001$. ****$p < 0.0001$, ns $p > 0.05$. Scale bar: 500 μm.

DPSCs ($p > 0.05$), with higher concentrations (DFO-40) demonstrating a stronger effect.

In the tube formation assays, more extensive blood-vessel network and complete tubular structures were found in the DPSC-DFO-40 group, indicating that DFO-GMSs hydrogel composite effectively promoted vascularization in vitro (Figure 4A). Furthermore, no significant variation was recorded between the DPSC-DFO-0 group and un-DPSC-DFO-0

https://doi.org/10.1021/acsomega.5c00445
ACS Omega 2025, 10, 12579−12589

group ($p > 0.05$), and DPSCs-DFO-40 group showed higher segments length compared with un-DPSC-DFO-40 group ($p < 0.05$), suggesting that DFO released from the hydrogel composite promoted vascularization by enhancing the secretion and levels of angiogenesis-related factors in DPSCs.

4. DISCUSSION

This study reported the successful synthesis of a GMSs hydrogel composite, with DFO incorporated into the material through encapsulation within GMSs. The drug release experiments demonstrated the potential of GMSs hydrogel composite to provide sustained release of the drug over 15 days. According to the experiments of Jiang, the concentration of DFO at 20 μM showed toxic effects on pulp cells, inhibiting the growth of DPSCs.[26] However, in the CCK-8 assays, DPSCs in the DFO-20 group retained high viability on day 3 and 5. This indicates the ability of the hydrogel composite to regulate drug release. While hydrogels generally have favorable biocompatibility, they can suffer from burst release and rapid diffusion of drugs. The incorporation of GMSs effectively slowed down the drug release, providing a more controlled delivery.[36]

DFO is a commonly used iron chelator in clinical hematology. It functions by binding to iron ions and preventing the degradation of HIF by proline hydroxylase, thereby activating the hypoxic signaling pathway even under normoxic conditions. It has been found that both topical and systemic administration of DFO promotes bone formation and vascularization, thereby enhancing the repair of bone defects while facilitating fracture healing.[37,38] However, owing to the limited half-life of DFO in the body, achieving local drug enrichment through oral administration is challenging. Furthermore, systemic application of DFO has been associated with adverse reactions resulting from overdose.[41] Recent research has focused on improving local DFO applications. Ding et al. combined DFO with silk nanofibers, demonstrating strong physical interaction with DFO, effectively avoiding the need for chemical cross-linking. DFO-loaded silk nanofiber hydrogel systems showed zero-order drug release over 40 days and promoted enhanced vascular network formation in wound sites.[39] Donneys et al. conjugated hyaluronic acid with DFO, enabling its immobilization within fracture-healing tissue while also providing sustained release of DFO for over 10 days, ensuring its activity during angiogenesis.[40] Li et al. introduce a composite hydrogel combining gelatin and hyaluronic acid (HA), with the encapsulation of DFO nanoparticles (DFO NPs). The DFO NPs showed a ustained release of DFO over 12 days and hydrogel Encapsulating the DFO NPs enabled controlled release over 15 days.[61] This is similar to our idea of improving microsphere mechanical properties and drug delivery by adding drug-carrying microspheres to hydrogels, but the materials used to fabricate the microspheres and hydrogels were different from ours, which may led to differences in the release of drug. In this study, DFO was found to be released over 15 days in vitro, facilitated by the combined effects of physical adsorption by GMSs and encapsulation within the hydrogel. Moreover, the porous structure of the hydrogel enhanced DPSCs adhesion, while the microsphere incorporation increased the hydrogel's surface area. Cytoskeletal staining revealed that the cells adopt a star- or shuttle-shaped morphology, with established intercellular connections.

With advancements in tissue engineering, significant progress has been accomplished in pulp regeneration. Tissue engineering is typically associated with the integration of stem cells, biomaterials, and bioactive growth factors.[1] DPSCs possess the potential for multilineage differentiation into odontoblasts, nerve cells, and endothelial cells (ECs), making them a promising candidate for pulp regeneration.[42,43] It has been reported that DPSCs promote angiogenesis in vivo, demonstrating vascular properties.[44] A recent study on canine partial pulp regeneration also observed the formation of blood vessel-like structures in the regenerated tissue. Gene expression analysis revealed the upregulation of proangiogenic factors, supporting the potential of DPSCs as a source of cells for complete pulp regeneration through angiogenesis and vasculogenesis.[45] To enhance vascularization, studies have combined stem cells from human exfoliated deciduous teeth with ECs. However, the results indicated no significant enhancement in microvessel density within the regenerated pulp. Instead, it is DPSCs themselves that show great angiogenic potential by secreting VEGF to support vascular morphogenesis, which can be further promoted by hypoxic pretreatment.[46]

The current study demonstrated that the DFO-GMSs hydrogel composite stimulated DPSCs to secrete angiogenesis-related factors, and enhancing angiogenesis in vitro. Liu et al. fabricated DFO-loaded hydrogel to control the release of DFO and observed DFO promoted the secretion of NO and VEGF from HUVECs.[62] Zhu et al. came to similar conclusions that DFO promoted the secretion of VEGF and HIF-1α.[63] In this study, we observed the same enhance of VEGF secretion from DPSCs by released DFO. The results suggest that DFO may have a similar promoting effect on DPSCs and HUVECs. Considering that the effect of DFO on HUVECs is mainly through a key signaling molecule HIF-1α,[64] whose secretion we also detected in our study using ELISA and qPCR, further studies may be needed to examine the relationship between the effect of DFO on DPSC and HIF-1α. The activation of HIF-1α signaling in DPSCs may be an essential pathway through which DFO exerts its biological effects.

HIF-1α is a cellular oxygen sensor. Under normoxic conditions, two proline residues in the central degradation domain of HIF-1α are hydroxylated by proline hydroxylases (PHDs) that require Fe^{2+}, leading to HIF-1α degradation.[47] Limiting oxygen or restricting the availability of Fe^{2+} through iron chelation prevents HIF-1α from undergoing proteolysis, thereby stabilizing and enhancing its activity.[48] Under hypoxic conditions, DPSCs frequently upregulate HIF-1α expression, which in turn promotes the increased expression of angiogenic genes, including VEGF, and FGF2.[13,14] VEGF, a target gene of HIF-1α, exerts a crucial role in angiogenesis. Under hypoxia, HIF-1α accumulation triggers VEGF activation, promoting angiogenesis with improved oxygen delivery.[49] HIF-1α and signal transducer of transcription 3 (STAT3) simultaneously bind to the VEGF promoter, forming complexes with transcriptional coactivators ref-1/APE and CBP/p300 to activate VEGF expression. The binding of HIF-1α and STAT3 to the VEGF promoter is crucial to maximal transcription of VEGF mRNA under hypoxia.[50] The HIF-1α/VEGF pathway may be a potential mechanism for promoting angiogenesis in DPSCs, which requires further experimental validation.

Moreover, HIF-1 is a key signaling molecule coupling osteogenesis and angiogenesis.[51,52] HIF-1α overexpression

https://doi.org/10.1021/acsomega.5c00445
ACS Omega 2025, 10, 12579−12589

activates the VEGF/AKT/mTOR signaling pathway, leading to increased levels of phosphorylated AKT (p-AKT) and phosphorylated mTOR (p-mTOR), thereby enhancing the osteogenic and angiogenic potential of adipose-derived stem cell (ADSC).[53] VEGF/AKT/mTOR pathway may participate in odontoblast differentiation in DPCs. After odontoblast induction, VEGF and AKT mRNA expression in DPCs increased dramatically.[54] Meanwhile, VEGF binds to the VEGF receptor (VEGFR) and p-AKT, thereby increasing the expression of p-AKT, which further activates endothelial nitric oxide synthase (eNOS).[55,56] eNOS, a key enzyme in NO production, plays a central role in modulating the expression of NO through the regulation of upstream signaling pathways.[57] NO promotes ECs proliferation and exerts significant vasodilatory effects.[58] The dual potential of DFO to promote angiogenesis and bone formation could provide valuable insights for pulp regeneration, but one major limitation of this study is the lack of in vivo experimental, which may affect the feasibility of DFO-GMSs hydrogel composite for practical applications. Future studies should consider collecting these data in order to further argue our point and thus more accurately assess the potential of the hydrogel composite in pulp regeneration.

5. CONCLUSIONS

The study reported the successful synthesis of DFO-GMSs hydrogel composite demonstrating significant physical properties with sustained and long-term drug release behavior. The drug delivery system enhanced the migration and secretion of angiogenesis-related factors (VEGF, HIF-1α, FGF2) in DPSCs, thereby promoting blood vessel formation. Furthermore, HIF-1α may play a crucial role in the blood vessels formation and the enhancement of dentin repair. Considering the strong relationship between angiogenesis and pulp regeneration, rapid revascularization is essential for effective pulp regeneration. Therefore, drugs or growth factors targeting angiogenesis may provide promising approaches for future treatments.

AUTHOR INFORMATION

Corresponding Author

Hongyan Zhang − *College and Hospital of Stomatology, Anhui Medical University, Key Lab. of Oral Diseases Research of Anhui Province, Hefei 230032, China*; Phone: +8618019984310; Email: toothyan@126.com

Authors

Jie Wang − *College and Hospital of Stomatology, Anhui Medical University, Key Lab. of Oral Diseases Research of Anhui Province, Hefei 230032, China*; orcid.org/0000-0001-6074-5985

Fan Yang − *College and Hospital of Stomatology, Anhui Medical University, Key Lab. of Oral Diseases Research of Anhui Province, Hefei 230032, China*

Ruting Chen − *College and Hospital of Stomatology, Anhui Medical University, Key Lab. of Oral Diseases Research of Anhui Province, Hefei 230032, China; Department of Stomatology, Yangjiang People's Hospital, Affiliated Yangjiang Hospital of Guangdong Medical University, Yangjiang 529500, China*

Xinyue Yang − *College and Hospital of Stomatology, Anhui Medical University, Key Lab. of Oral Diseases Research of Anhui Province, Hefei 230032, China*

Jingjing Wang − *College and Hospital of Stomatology, Anhui Medical University, Key Lab. of Oral Diseases Research of Anhui Province, Hefei 230032, China*

Complete contact information is available at: https://pubs.acs.org/10.1021/acsomega.5c00445

Funding

This work was supported by the Natural Science Foundation of Universities of Anhui province (KJ2020A0165), Research improvement program in Stomatologic Hospital and College of Anhui Medical University (No. 2023xkfyts04, 2022xkfyts10).

Notes

This study strictly adhered to the requirements of the Declaration of Helsinki. It was approved by the Ethics Committee of the Affiliated Stomatological Hospital of Anhui Medical University (T2024037).

The authors declare no competing financial interest.

ACKNOWLEDGMENTS

J.W.: Conception and design, acquisition of data, analysis and interpretation of data, drafting the article. F.Y. and R.C.: Analysis and interpretation of data, drafting the article. X.Y. and J.W.: Acquisition and analysis of data. H.Z.: Conception and design, revising the article and final approval. All authors read and approved the final manuscript.

REFERENCES

(1) Xie, Z.; Shen, Z.; Zhan, P.; Yang, J.; Huang, Q.; Huang, S.; Chen, L.; Lin, Z. Functional Dental Pulp Regeneration: Basic Research and Clinical Translation. *Int. J. Mol. Sci.* **2021**, *22* (16), 8991.

(2) Xu, X.; Liang, C.; Gao, X.; Huang, H.; Xing, X.; Tang, Q.; Yang, J.; Wu, Y.; Li, M.; Li, H.; Liao, L.; Tian, W. Adipose Tissue-derived Microvascular Fragments as Vascularization Units for Dental Pulp Regeneration. *J. Endod.* **2021**, *47* (7), 1092−1100.

(3) Chen, J.; Xu, H.; Xia, K.; Cheng, S.; Zhang, Q. Resolvin E1 accelerates pulp repair by regulating inflammation and stimulating dentin regeneration in dental pulp stem cells. *Stem Cell Res. Ther.* **2021**, *12* (1), 75.

(4) Tsutsui, T. W. Dental Pulp Stem Cells: Advances to Applications. Stem Cells. *Cloning* **2020**, *13*, 33−42.

(5) Ziauddin, S. M.; Nakashima, M.; Watanabe, H.; Tominaga, M.; Iohara, K. Biological characteristics and pulp regeneration potential of stem cells from canine deciduous teeth compared with those of permanent teeth. *Stem Cell Res. Ther.* **2022**, *13* (1), 439.

(6) Yang, J. W.; Zhang, Y. F.; Sun, Z. Y.; Song, G. T.; Chen, Z. Dental pulp tissue engineering with bFGF-incorporated silk fibroin scaffolds. *J. Biomater. Appl.* **2015**, *30* (2), 221−229.

(7) Zhu, L.; Dissanayaka, W. L.; Zhang, C. Dental pulp stem cells overexpressing stromal-derived factor-1α and vascular endothelial growth factor in dental pulp regeneration. *Clin. Oral Investig.* **2019**, *23* (5), 2497−2509.

(8) Zhang, M.; Jiang, F.; Zhang, X.; Wang, S.; Jin, Y.; Zhang, W.; Jiang, X. The Effects of Platelet-Derived Growth Factor-BB on Human Dental Pulp Stem Cells Mediated Dentin-Pulp Complex Regeneration. *Stem Cells Transl. Med.* **2023**, *12* (5), 322−323.

(9) Saghiri, M. A.; Asatourian, A.; Sorenson, C. M.; Sheibani, N. Role of angiogenesis in endodontics: contributions of stem cells and proangiogenic and antiangiogenic factors to dental pulp regeneration. *J. Endod.* **2015**, *41* (6), 797−803.

(10) Nowak-Stępniowska, A.; Osuchowska, P. N.; Fiedorowicz, H.; Trafny, E. A. Insight in Hypoxia-Mimetic Agents as Potential Tools for Mesenchymal Stem Cell Priming in Regenerative Medicine. *Stem Cells Int.* **2022**, *2022*, No. 8775591.

(11) Grewal, B. S.; Keller, B.; Weinhold, P.; Dahners, L. E. Evaluating effects of deferoxamine in a rat tibia critical bone defect model. *J. Orthop.* **2014**, *11* (1), 5−9.
(12) Fujisawa, K.; Takami, T.; Okada, S.; Hara, K.; Matsumoto, T.; Yamamoto, N.; Yamasaki, T.; Sakaida, I. Analysis of Metabolomic Changes in Mesenchymal Stem Cells on Treatment with Desferrioxamine as a Hypoxia Mimetic Compared with Hypoxic Conditions. *Stem Cells* **2018**, *36* (8), 1226−1236.
(13) Zhang, J.; Tong, D.; Song, H.; Ruan, R.; Sun, Y.; Lin, Y.; Wang, J.; Hou, L.; Dai, J.; Ding, J.; Yang, H. Osteoimmunity-Regulating Biomimetically Hierarchical Scaffold for Augmented Bone Regeneration. *Adv. Mater.* **2022**, *34* (36), No. e2202044.
(14) Zeng, Y.; Huang, C.; Duan, D.; Lou, A.; Guo, Y.; Xiao, T.; Wei, J.; Liu, S.; Wang, Z.; Yang, Q.; Zhou, L.; Wu, Z.; Wang, L. Injectable temperature-sensitive hydrogel system incorporating deferoxamine-loaded microspheres promotes H-type blood vessel-related bone repair of a critical size femoral defect. *Acta Biomater.* **2022**, *153*, 108−123.
(15) Holden, P.; Nair, L. S. Deferoxamine: An Angiogenic and Antioxidant Molecule for Tissue Regeneration. *Tissue Eng. Part B Rev.* **2019**, *25* (6), 461−470.
(16) Ran, Q.; Yu, Y.; Chen, W.; Shen, X.; Mu, C.; Yuan, Z.; Tao, B.; Hu, Y.; Yang, W.; Cai, K. Deferoxamine loaded titania nanotubes substrates regulate osteogenic and angiogenic differentiation of MSCs via activation of HIF-1α signaling. *Mater. Sci. Eng. C Mater. Biol. Appl.* **2018**, *91*, 44−54.
(17) Shi, R.; Zhang, J.; Niu, K.; Li, W.; Jiang, N.; Li, J.; Yu, Q.; Wu, C. Electrospun artificial periosteum loaded with DFO contributes to osteogenesis via the TGF-β1/Smad2 pathway. *Biomater. Sci.* **2021**, *9* (6), 2090−2102.
(18) Yan, Y.; Chen, H.; Zhang, H.; Guo, C.; Yang, K.; Chen, K.; Cheng, R.; Qian, N.; Sandler, N.; Zhang, Y. S.; Shen, H.; Qi, J.; Cui, W.; Deng, L. Vascularized 3D printed scaffolds for promoting bone regeneration. *Biomaterials* **2019**, *190*−*191*, 97−110.
(19) Oses, C.; Olivares, B.; Ezquer, M.; Acosta, C.; Bosch, P.; Donoso, M.; Léniz, P.; Ezquer, F. Preconditioning of adipose tissue-derived mesenchymal stem cells with deferoxamine increases the production of pro-angiogenic, neuroprotective and anti-inflammatory factors: Potential application in the treatment of diabetic neuropathy. *PloS One* **2017**, *12* (5), No. e0178011.
(20) Xu, L.; Guan, R.; Yu, B.; Li, Y.; Liu, H.; Jiang, Y. Fluorene methoxycarbonyl-PEG-deferoxamine conjugates "hitchhike" with albumin in situ for iron overload therapy. *Int. J. Pharm.* **2022**, *625*, No. 122136.
(21) Wang, Y.; Liu, Z.; Lin, T. M.; Chanana, S.; Xiong, M. P. Nanogel-DFO conjugates as a model to investigate pharmacokinetics, biodistribution, and iron chelation in vivo. *Int. J. Pharm.* **2018**, *538* (1−2), 79−86.
(22) Lazaridou, M.; Christodoulou, E.; Nerantzaki, M.; Kostoglou, M.; Lambropoulou, D. A.; Katsarou, A.; Pantopoulos, K.; Bikiaris, D. N. Formulation and In-Vitro Characterization of Chitosan-Nanoparticles Loaded with the Iron Chelator Deferoxamine Mesylate (DFO). *Pharmaceutics.* **2020**, *12* (3), 238.
(23) Shen, H.; Zhang, C.; Meng, Y.; Qiao, Y.; Ma, Y.; Chen, J.; Wang, X.; Pan, L. Biomimetic Hydrogel Containing Copper Sulfide Nanoparticles and Deferoxamine for Photothermal Therapy of Infected Diabetic Wounds. *Adv. Healthc Mater.* **2024**, *13* (8), No. e2303000.
(24) Mu, S.; Guo, S.; Wang, X.; Zhan, Y.; Li, Y.; Jiang, Y.; Zhang, R.; Zhang, B. Effects of deferoxamine on the osteogenic differentiation of human periodontal ligament cells. *Mol. Med. Rep.* **2017**, *16* (6), 9579−9586.
(25) Du, R.; Zhao, J.; Wen, Y.; Zhu, Y.; Jiang, L. Deferoxamine enhances the migration of dental pulp cells via hypoxia-inducible factor 1α. *Am. J. Transl. Res.* **2021**, *13* (5), 4780−4787.
(26) Jiang, L.; Peng, W. W.; Li, L. F.; Du, R.; Wu, T. T.; Zhou, Z. J.; Zhao, J. J.; Yang, Y.; Qu, D. L.; Zhu, Y. Q. Effects of deferoxamine on the repair ability of dental pulp cells in vitro. *J. Endod.* **2014**, *40* (8), 1100−1104.
(27) Lee, K. E.; Mo, S.; Lee, H. S.; Jeon, M.; Song, J. S.; Choi, H. J.; Cho, H.; Kang, C. M. Deferoxamine Reduces Inflammation and Osteoclastogenesis in Avulsed Teeth. *Int. J. Mol. Sci.* **2021**, *22* (15), 8225.
(28) Zheng, L.; Liu, Y.; Jiang, L.; Wang, X.; Chen, Y.; Li, L.; Song, M.; Zhang, H.; Zhang, Y. S.; Zhang, X. Injectable decellularized dental pulp matrix-functionalized hydrogel microspheres for endodontic regeneration. *Acta Biomater.* **2023**, *156*, 37−48.
(29) Long, T.; Tan, W.; Tian, X.; Tang, Z.; Hu, K.; Ge, L.; Mu, C.; Li, X.; Xu, Y.; Zhao, L.; Li, D. Gelatin/alginate-based microspheres with sphere-in-capsule structure for spatiotemporal manipulative drug release in gastrointestinal tract. *Int. J. Biol. Macromol.* **2023**, *226*, 485−495.
(30) Cao, H.; Duan, L.; Zhang, Y.; Cao, J.; Zhang, K. Current hydrogel advances in physicochemical and biological response-driven biomedical application diversity. *Signal Transduct Target Ther.* **2021**, *6* (1), 426.
(31) Zheng, Y.; Wang, W.; Zhao, J.; Wu, C.; Ye, C.; Huang, M.; Wang, S. Preparation of injectable temperature-sensitive chitosan-based hydrogel for combined hyperthermia and chemotherapy of colon cancer. *Carbohydr. Polym.* **2019**, *222*, No. 115039.
(32) Kilmer, C. E.; Battistoni, C. M.; Cox, A.; Breur, G. J.; Panitch, A.; Liu, J. C. Collagen Type I and II Blend Hydrogel with Autologous Mesenchymal Stem Cells as a Scaffold for Articular Cartilage Defect Repair. *ACS Biomater. Sci. Eng.* **2020**, *6* (6), 3464−3476.
(33) Hesse, E.; Hefferan, T. E.; Tarara, J. E.; Haasper, C.; Meller, R.; Krettek, C.; Lu, L.; Yaszemski, M. J. Collagen type I hydrogel allows migration, proliferation, and osteogenic differentiation of rat bone marrow stromal cells. *J. Biomed. Mater. Res. A* **2010**, *94* (2), 442−449.
(34) Nouri-Felekori, M.; Khakbiz, M.; Nezafati, N.; Mohammadi, J.; Eslaminejad, M. B. Comparative analysis and properties evaluation of gelatin microspheres crosslinked with glutaraldehyde and 3-glycidoxypropyltrimethoxysilane as drug delivery systems for the antibiotic vancomycin. *Int. J. Pharm.* **2019**, *557*, 208−220.
(35) Yoshinari, M.; Hayakawa, T.; Matsuzaka, K.; Inoue, T.; Oda, Y.; Shimono, M.; Ide, T.; Tanaka, T. Oxygen plasma surface modification enhances immobilization of simvastatin acid. *Biomed. Res.* **2006**, *27* (1), 29−36.
(36) Gao, W.; Zhang, Y.; Zhang, Q.; Zhang, L. Nanoparticle-Hydrogel: A Hybrid Biomaterial System for Localized Drug Delivery. *Ann. Biomed. Eng.* **2016**, *44* (6), 2049−2061.
(37) Jia, P.; Chen, H.; Kang, H.; Qi, J.; Zhao, P.; Jiang, M.; Guo, L.; Zhou, Q.; Qian, N. D.; Zhou, H. B.; Xu, Y. J.; Fan, Y.; Deng, L. F. Deferoxamine released from poly(lactic-co-glycolic acid) promotes healing of osteoporotic bone defect via enhanced angiogenesis and osteogenesis. *J. Biomed Mater. Res. A* **2016**, *104* (10), 2515−2527.
(38) Wang, L.; Jia, P.; Shan, Y.; Hao, Y.; Wang, X.; Jiang, Y.; Yuan, Y.; Du, Q.; Zhang, H.; Yang, F.; Zhang, W.; Sheng, M.; Xu, Y. Synergistic protection of bone vasculature and bone mass by desferrioxamine in osteoporotic mice. *Mol. Med. Rep.* **2017**, *16* (5), 6642−6649.
(39) Ding, Z.; Zhou, M.; Zhou, Z.; Zhang, W.; Jiang, X.; Lu, X.; Zuo, B.; Lu, Q.; Kaplan, D. L. Injectable Silk Nanofiber Hydrogels for Sustained Release of Small-Molecule Drugs and Vascularization. *ACS Biomater. Sci. Eng.* **2019**, *5* (8), 4077−4088.
(40) Donneys, A.; Yang, Q.; Forrest, M. L.; Nelson, N. S.; Zhang, T.; Ettinger, R.; Ranganathan, K.; Snider, A.; Deshpande, S. S.; Cohen, M. S.; Buchman, S. R. Implantable hyaluronic acid-deferoxamine conjugate prevents nonunions through stimulation of neovascularization. *NPJ Regen. Med.* **2019**, *4*, 11.
(41) Botzenhardt, S.; Li, N.; Chan, E. W.; Sing, C. W.; Wong, I. C.; Neubert, A. Safety profiles of iron chelators in young patients with haemoglobinopathies. *Eur. J. Haematol.* **2017**, *98* (3), 198−217.
(42) Xuan, K.; Li, B.; Guo, H.; Sun, W.; Kou, X.; He, X.; Zhang, Y.; Sun, J.; Liu, A.; Liao, L.; Liu, S.; Liu, W.; Hu, C.; Shi, S.; Jin, Y. Deciduous autologous tooth stem cells regenerate dental pulp after implantation into injured teeth. *Sci. Transl. Med.* **2018**, *10* (455), No. eaaf3227.

https://doi.org/10.1021/acsomega.5c00445
ACS Omega 2025, 10, 12579−12589

(43) Lee, H. N.; Liang, C.; Liao, L.; Tian, W. D. Advances in Research on Stem Cell-Based Pulp Regeneration. Tissue Eng. *Regen. Med.* **2021**, *18* (6), 931−940.
(44) Sui, B.; Wu, D.; Xiang, L.; Fu, Y.; Kou, X.; Shi, S. Dental Pulp Stem Cells: From Discovery to Clinical Application. *J. Endod.* **2020**, *46* (9S), S46−S55.
(45) Iohara, K.; Zheng, L.; Ito, M.; Ishizaka, R.; Nakamura, H.; Into, T.; Matsushita, K.; Nakashima, M. Regeneration of dental pulp after pulpotomy by transplantation of CD31(−)/CD146(−) side population cells from a canine tooth. *Regen. Med.* **2009**, *4* (3), 377−385.
(46) Cordeiro, M. M.; Dong, Z.; Kaneko, T.; Zhang, Z.; Miyazawa, M.; Shi, S.; Smith, A. J.; Nör, J. E. Dental pulp tissue engineering with stem cells from exfoliated deciduous teeth. *J. Endod.* **2008**, *34* (8), 962−969.
(47) Jones, D. T.; Harris, A. L. Identification of novel small-molecule inhibitors of hypoxia-inducible factor-1 transactivation and DNA binding. *Mol. Cancer Ther.* **2006**, *5* (9), 2193−2202.
(48) Kusumbe, A. P.; Ramasamy, S. K.; Adams, R. H. Coupling of angiogenesis and osteogenesis by a specific vessel subtype in bone. *Nature.* **2014**, *513* (7519), 574.
(49) Ahluwalia, A.; Tarnawski, A. S. Critical role of hypoxia sensor−HIF-1α in VEGF gene activation. Implications for angiogenesis and tissue injury healing. *Curr. Med. Chem.* **2012**, *19* (1), 90−97.
(50) Gray, M. J.; Zhang, J.; Ellis, L. M.; Semenza, G. L.; Evans, D. B.; Watowich, S. S.; Gallick, G. E. HIF-1alpha, STAT3, CBP/p300 and Ref-1/APE are components of a transcriptional complex that regulates Src-dependent hypoxia-induced expression of VEGF in pancreatic and prostate carcinomas. *Oncogene* **2005**, *24* (19), 3110−3120.
(51) Zhang, Y.; Huang, J.; Wang, C.; Zhang, Y.; Hu, C.; Li, G.; Xu, L. Application of HIF-1α by gene therapy enhances angiogenesis and osteogenesis in alveolar bone defect regeneration. *J. Gene Med.* **2016**, *18* (4−6), 57−64.
(52) Bai, H.; Wang, Y.; Zhao, Y.; Chen, X.; Xiao, Y.; Bao, C. HIF signaling: A new propellant in bone regeneration. *Biomater. Adv.* **2022**, *138*, No. 212874.
(53) Song, S.; Zhang, G.; Chen, X.; Zheng, J.; Liu, X.; Wang, Y.; Chen, Z.; Wang, Y.; Song, Y.; Zhou, Q. HIF-1α increases the osteogenic capacity of ADSCs by coupling angiogenesis and osteogenesis via the HIF-1α/VEGF/AKT/mTOR signaling pathway. *J. Nanobiotechnol.* **2023**, *21* (1), 257.
(54) Liu, Z.; Chen, T.; Han, Q.; Chen, M.; You, J.; Fang, F.; Peng, L.; Wu, B. HDAC inhibitor LMK-235 promotes the odontoblast differentiation of dental pulp cells. *Mol. Med. Rep.* **2018**, *17* (1), 1445−1452.
(55) Gentile, C.; Muise-Helmericks, R. C.; Drake, C. J. VEGF-mediated phosphorylation of eNOS regulates angioblast and embryonic endothelial cell proliferation. *Dev. Biol.* **2013**, *373* (1), 163−175.
(56) Yu, M.; Liu, W.; Li, J.; Lu, J.; Lu, H.; Jia, W.; Liu, F. Exosomes derived from atorvastatin-pretreated MSC accelerate diabetic wound repair by enhancing angiogenesis via AKT/eNOS pathway. *Stem Cell Res. Ther.* **2020**, *11* (1), 350.
(57) Zheng, Y.; Wang, J.; Zhao, T.; Wang, L.; Wang, J. Modulation of the VEGF/AKT/eNOS signaling pathway to regulate liver angiogenesis to explore the anti-hepatic fibrosis mechanism of curcumol. *J. Ethnopharmacol.* **2021**, *280*, No. 114480.
(58) Dudzinski, D. M.; Michel, T. Life history of eNOS: partners and pathways. *Cardiovasc. Res.* **2007**, *75* (2), 247−260.
(59) Lan, Y.; Li, W.; Jiao, Y.; Guo, R.; Zhang, Y.; Xue, W.; Zhang, Y. Therapeutic efficacy of antibiotic-loaded gelatin microsphere/silk fibroin scaffolds in infected full-thickness burns. *Acta Biomater.* **2014**, *10* (7), 3167−3176.
(60) Kudva, A. K.; Dikina, A. D.; Luyten, F. P.; Alsberg, E.; Patterson, J. Gelatin microspheres releasing transforming growth factor drive in vitro chondrogenesis of human periosteum derived cells in micromass culture. *Acta Biomater.* **2019**, *90*, 287−299.
(61) Li, J.; Lu, X.; Weng, M.; Wang, Y.; Tang, J.; Xu, Q.; Zhang, L.; Bai, J. Promoting tissue repair using deferoxamine nanoparticles loaded biomimetic gelatin/HA composite hydrogel. *Biomed Mater.* **2024**, *19* (4), No. ad46ba.
(62) Liu, H.; Li, K.; Yi, D.; Ding, Y.; Gao, Y.; Zheng, X. Deferoxamine-Loaded Chitosan-Based Hydrogel on Bone Implants Showing Enhanced Bond Strength and Pro-Angiogenic Effects. *J. Funct Biomater.* **2024**, *15* (4), 112.
(63) Zhu, Y.; Shi, Z.; Pang, Y.; Zhou, Y. Deferoxamine-loaded gelatin methacryloyl hydrogel endue 3D-printed PGCL-hydroxyapatite scaffold with angiogenesis, anti-oxidative and immunoregulatory capacities for facilitating bone healing. *Int. J. Biol. Macromol.* **2025**, *3* (295), No. 139509.
(64) Hou, Z.; Nie, C.; Si, Z.; Ma, Y. Deferoxamine enhances neovascularization and accelerates wound healing in diabetic rats via the accumulation of hypoxia-inducible factor-1α. *Diabetes Res. Clin. Pract.* **2013**, *101* (1), 62−71.
(65) Hamilton, J. L.; Ul-Haq, M. I.; Creagh, A. L.; Haynes, C. A.; Kizhakkedathu, J. N. Iron Binding and Iron Removal Efficiency of Desferrioxamine Based Polymeric Iron Chelators: Influence of Molecular Size and Chelator Density. *Macromol. Biosci.* **2017**, *17* (3), No. 1600244.
(66) Mushtaq, F.; Raza, Z. A.; Batool, S. R.; Zahid, M.; Onder, O. C.; Rafique, A.; Nazeer, M. A. Preparation, properties, and applications of gelatin-based hydrogels (GHs) in the environmental, technological, and biomedical sectors. *Int. J. Biol. Macromol.* **2022**, *218*, 601−633.
(67) Chen, S.; Wang, Y.; Lai, J.; Tan, S.; Wang, M. Structure and Properties of Gelatin Methacryloyl (GelMA) Synthesized in Different Reaction Systems. *Biomacromolecules* **2023**, *24* (6), 2928−2941.

https://doi.org/10.1021/acsomega.5c00445
ACS Omega 2025, 10, 12579−12589